Determination of the excited-state structure of 7-azaindole-water cluster using a Franck-Condon analysis

Robert Brause, Daniel Krügler,[a] Michael Schmitt, and Karl Kleinermanns[b]
Institut für Physikalische Chemie, Heinrich-Heine-Universität, D-40225 Düsseldorf, Germany

Atsushi Nakajima
Department of Chemistry, Faculty of Science and Technology, Keio University, 3-14-1 Hiyoshi, Kohoku-ku, Yokohama 223-8522, Japan

Terry A. Miller
Department of Chemistry, The Ohio State University, Columbus, Ohio 43210

(Received 2 August 2005; accepted 20 October 2005; published online 14 December 2005)

The change of the 7-azaindole-water cluster structure upon electronic excitation was determined by a Franck-Condon analysis of the intensities in the fluorescence emission spectra obtained via excitation of five different vibronic bands. A total of 105 emission band intensities were fitted, together with the changes of rotational constants of one isotopomer. These rotational constants have been obtained from a fit to the rovibronic contour of the cluster. The geometry change upon electronic excitation to the $\pi\pi^*$ state can be described by a strong and asymmetric shortening of the hydrogen bonds and a deformation of both the pyridine and the pyrrole rings of 7-azaindole. The resulting geometry changes are interpreted on the basis of *ab initio* calculations. © *2005 American Institute of Physics*. [DOI: 10.1063/1.2136868]

I. INTRODUCTION

Compared with the vast literature about the geometries of molecules in their electronic ground states, relatively little is known about their structures in electronically excited states. This is due to the fact that standard methods for structure determination, such as x-ray or neutron diffraction or microwave spectroscopy, cannot be applied to electronically excited states. Methodical exceptions are rotationally resolved laser-induced fluorescence spectroscopy, its resonant ionization variant, and rotational coherence spectroscopy. All three methods give the inertial parameters of the investigated molecules for the ground state and the electronically excited state. Already in medium-sized molecules, the number of structural parameters exceeds the number of inertial constants by far. Thus isotopic species of the parent substance have to be utilized to overcome this problem. Owing to the immense experimental effort a sufficient number of different isotopomers for a complete or nearly complete structure determination in both electronic states were used only in few studies.[1]

An alternative approach to excited-state structures is facilitated by the Franck-Condon (FC) principle. According to the FC principle the probability of a vibronic transition and thus the relative intensity of a vibronic band depends on the overlap integral of the vibrational wave functions of both electronic states. This overlap integral is determined by the relative shift of the two potential-energy curves connected by the vibronic transition along the normal coordinates Q of both states,

$$\mathrm{FC} = \left| \int [\Psi'(Q')]^* \Psi''(Q'') dQ' \right|^2 = \langle v' \cdots v'_N | v'' \cdots v''_N \rangle^2, \tag{1}$$

where the $\Psi(Q)$ are the N-dimensional vibrational wave functions. The normal coordinates Q' of the excited state and Q'' of the ground state are related by the linear orthogonal transformation given by Duschinsky.[2]

Thus, via the calculated FC factors the structural change upon electronic excitation can be deduced from the experimentally determined intensity pattern. A fit of the geometry change to the observed intensity pattern requires an efficient algorithm to compute all FC factors that are necessary. We use the recursive relation given by Doktorov *et al.*[3,4] to calculate the FC factors in the harmonic approximation. We presented a computer program which is able to perform fits of the intensity distributions in fluorescence emission spectra and of the changes of rotational constants of selected isotopomers.[5] In this paper the underlying theoretical basics of the calculation of the integrals in Eq. (1) and the fitting procedure are presented.

Kim and Bernstein[6] presented mass-resolved excitation spectra of 7-azaindole and its clusters with Ar, CH_4, NH_3, H_2O, D_2O, CH_3OH, and C_2H_5OH. They analyzed the obtained spectra with regard to monomer and cluster geometry. For the azaindole-water cluster they deduced a structure in which the water moiety is bonded to the π system instead of a hydrogen-bonded structure.

Fuke *et al.*[7] measured mass-resolved ionization spectra and fluorescence excitation spectra of 7-azaindole, 7-azaindole$(H_2O)_{1,2}$, and (7-azaindole)$_2$. From the large spec-

[a]Present address: Bruker-Daltonik GmbH, 28359 Bremen, Germany.
[b]Electronic mail: kleinermanns@uni-duesseldorf.de

tral redshift (1285 cm^{-1}) they proposed a considerable distortion of the geometry upon electronic excitation of the water clusters.

Nakajima *et al.*[8] investigated the geometric structures of 7-azaindole$(H_2O)_{1-3}$ and of the 7-azaindole dimer using laser-induced fluorescence spectroscopy with high resolution ($\sim$0.01 cm^{-1}). They deduced a planar structure of the complex 7-azaindole$(H_2O)_1$ from the rotational analysis of the spectrum and *ab initio* calculations.

Yokoyama *et al.* studied 7-azaindole-water clusters by IR dip spectroscopy and *ab initio* molecular-orbital calculations.[9] They postulated a hydrogen-bonded ring structure for all 7-azaindole-water clusters.

In a preceding paper we determined the geometry changes of 7-azaindole monomer upon electronic excitation via a Franck-Condon fit of the emission line intensities from dispersed fluorescence spectra combined with a fit of the changes of the rotational constants of four isotopomers.[10]

II. EXPERIMENTAL AND COMPUTATIONAL DETAILS

The experimental setup for the dispersed fluorescence spectroscopy is described in detail in Ref. 11 and 12. In brief, 7-azaindole was evaporated at 410 K and coexpanded through a pulsed nozzle with a 500 μm orifice (General Valve) into the vacuum chamber using a mixture of helium flowed over water as carrier gas. To avoid the formation of bigger water cluster the water was kept at temperatures below the melting point (268 K). The output of a Nd:Yttrium aluminum garnet (YAG) (Spectra Physics, Quanta Ray Indi)-pumped dye laser (Lambda-Physik, FL3002) was frequency doubled and crossed perpendicularly with the molecular beam. The fluorescence light was collected perpendicularly to laser and molecular beams and was imaged on the entrance slit of a 1 m monochromator (Jobin Yvon, grating with 2400 grooves/mm blazed at 400 nm for first order). The entrance slit was varied between 10 and 50 μm, depending on the intensity of the pumped band. The dispersed fluorescence (DF) was recorded by an intensified charge-coupled device (CCD) camera (Flamestar II, LaVision). One dispersed fluorescence spectrum was obtained by summing the signal of 200 laser pulses and subtracting the background that emerges from scattered light. Fifty of these single spectra are summed up for a better signal/noise. This allows imaging a DF spectrum of about 600 cm^{-1} simultaneously. Accordingly, the relative intensities in our DF spectra do not vary with laser power. Only the intensity of the excited band is perturbed by scattered light. Thus, we normalize relative intensities with respect to the strongest band in the spectrum other than the resonance fluorescence band. The intensity uncertainty of the whole detection system (including grating, CCD chip, etc.) was checked by shifting a particular fluorescence line over the CCD chip by changing the grating position. The line intensity was monitored as a function of its position on the chip. This procedure was repeated for a number of fluorescence bands. The observed intensity error was 10% at maximum.

Ab initio calculations at the Møller-Plesset second-order perturbation theory (MP2) level of theory have been carried out using the GAUSSIAN 03 program package (revision b.04).[13] The self-consistent-field (SCF) convergence criterion used throughout the calculations was an energy change below 10^{-8} hartree, and a convergence criterion for the gradient optimization of the molecular geometry of $\partial E/\partial r < 1.5 \times 10^{-5}$ hartree/bohr and of $\partial E/\partial \varphi < 1.5 \times 10^{-5}$ hartree/deg respectively. Dunnings correlation consistent polarized valence double ζ basis set[14] (cc-pVDZ) was used for the MP2 calculations.

Ab initio calculations with density-functional theory (DFT) and with time-dependent density-functional theory (TDDFT) using the B3LYP functional (this functional differs from the B3LYP functional used in GAUSSIAN 03 by the correlation functional; here the VWN(V) is used while GAUSSIAN 03 has the VWN(III) functional implemented) were performed using the TURBOMOLE program package (version 5.7.1).[15–20] Dunnings correlation consistent polarized valence triple ζ basis set[14] (cc-pVTZ) was used for the (TD)DFT calculations.

Complete active space self-consistent-field (CASSCF) calculations were performed with the MOLCAS program package (version 6.0) (Ref. 21) for the ground as well as the first excited state. The complete π space (10,9) of the monomer including the lone pair of the N1 atom with correct π symmetry was utilized as active space with the cc-pVDZ basis set. One lone pair, localized at the oxygen atom of the water moiety with near π symmetry, was discarded, due to its low energy.

TABLE I. S_0-state geometry parameters calculated at the B3LYP/c-pVTZ, MP2/cc-pVDZ, and CASSCF/cc-pVDZ levels of theory. The atomic numbering refers to Fig. 1. All bond lengths are given in pm.

S_0	B3LYP	MP2	CAS(10,9)	Expt.
A''/MHz	1775	1784	1780	1751
B''/MHz	1349	1333	1288	1337
C''/MHz	768	765	749	759
ΔI/u Å^2	−1.3	−0.9	−1.6	−1.1
H1–O8	206.2	194.6	214.4	
N7–H7	196.9	199.4	217.3	
N1–C2	137.6	137.6	137.5	
C2–C3	136.9	139.3	137.0	
C3–C3*a*	143.1	143.3	144.2	
C3*a*–C7*a*	142.2	143.4	141.4	
C7*a*–N1	136.7	137.4	136.3	
C3*a*–C4	139.5	141.3	140.1	
C4–C5	138.8	139.8	139.2	
C5–C6	140.0	141.8	140.7	
C6–N7	133.3	134.6	133.1	
N7–C7*a*	133.1	134.8	133.1	
N1–H	101.4	102.7	100.1	
C2–H	107.7	109.2	107.7	
C3–H	107.7	108.8	107.7	
C4–H	108.3	109.5	108.2	
C5–H	108.1	109.5	108.1	
C6–H	108.3	109.6	108.2	
O8–H7	97.9	98.1	95.4	
O8–H8	96.1	96.7	94.7	

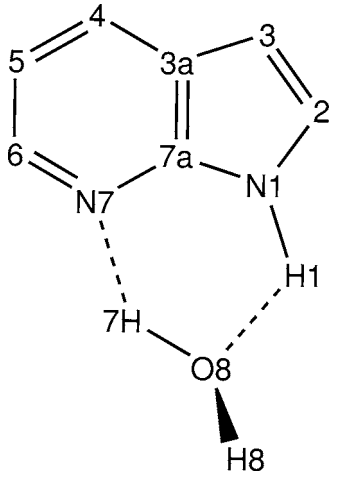

FIG. 1. Atomic numbering of 7AI-water cluster (1H-pyrrolo[2,3-*b*]pyridine water cluster).

Additionally, we performed CASPT2 single-point calculations on the optimized CASSCF and (TD)DFT structures. The calculations were performed on a SGI Origin2000 (MOLCAS), a Sun Fire 15 K (GAUSSIAN 03), and a Sun Opteron cluster (TURBOMOLE).

III. RESULTS

A. *Ab initio* calculations

The ground-state structure of the 7AI-water cluster was optimized at the MP2/cc-pVDZ, B3LYP/cc-pVTZ, and CASSCF(10,9)/cc-pVDZ levels of theory. The harmonic vibrational frequencies were calculated, using the analytical/numerical second derivatives of the potential energy. The MP2 vibrational frequencies were recalculated using the third derivatives to correct for the anharmonicity of some normal modes, especially of the intermolecular ones.

The resulting geometry parameters are presented in Table I. The atomic numbering in Table I refers to Fig. 1.

Table II presents the vibrational frequencies of the 48 normal modes of 7AI-water cluster calculated at the MP2/cc-pVDZ level of theory. Six intermolecular normal modes arise from complexation of 7AI with water. The numbering of the intermolecular modes follows the nomenclature of Schütz *et al.*[22] and the numbering of the intramolecular modes follows the nomenclature of Varsanyi[23] for ortho-di-light-substituted benzene derivatives, completed for vibrations of the five-membered ring.[12] As the 7AI-water cluster is a quite unsymmetrical molecule, the numbering scheme is not always unique and has to be taken as a rough description of the mode. The respective vibration should be inspected as animated graphs with a viewer such as MOLDEN or MOLEKEL.[24,25] The Gaussian.log file, the Turbomole.molf file as well as the MOLCAS.freq file, which contain the normal-mode analysis, can be downloaded from our homepage (http://www-public.rz.uni-duesseldorf.de/~pc1). The quoted calculated frequencies are unscaled and compared to the experimental frequencies in Table II. In the region between 1350 and 1550 cm^{-1} and in the range of the CH stretching vibrations, the spectra are too dense to allow a straightforward vibrational assignment.

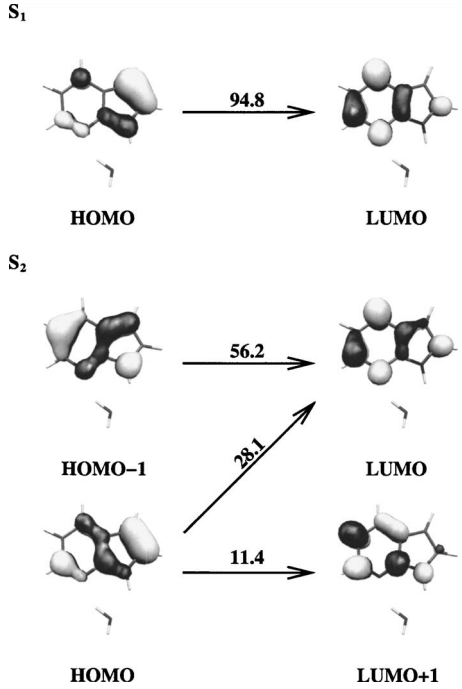

FIG. 2. Weights of the TDDFT molecular Kohn-Sham orbitals that are involved in the two lowest $\pi\pi^*$ transition. The orbitals are ordered by their energy.

The vertical and adiabatic excitation energies for the two lowest $\pi\pi^*$ transitions have been calculated at the CASSCF(10,9)/cc-pVDZ, the TDDFT B3LYP/cc-pVTZ, and the CASPT2(10,9)/cc-pVDZ level, using the CASSCF and (TD)DFT optimized structures. Table III reports excitation energies for both transitions. The experimentally determined vibrationless electronic origin ($S_1 \leftarrow S_0$) of 7AI-water cluster is at 33 340 cm^{-1} (4.13 eV), in good agreement with the adiabatic CASPT2(10,9)/cc-pVDZ transition energy of 32 436 cm^{-1} (4.02 eV) (CASPT2 using the CASSCF optimized S_1 geometry), the adiabatic CASPT2(10,9)/cc-pVDZ transition energy of 34 114 cm^{-1} (4.23 eV) (CASPT2 using the TDDFT optimized S_1 geometry), and the adiabatic TDDFT transition energy of 32 360 cm^{-1} (387 kJ/mol and 4.01 eV). The transition to the next $\pi\pi^*$ state (^1L_b) is calculated (CASPT2 using the TDDFT optimized S_2 geometry) to be ca. 1300 cm^{-1} (0.16 eV) higher in energy. The CASPT2 results for the excitation energy show that the TDDFT method gets the ^1L_a state energy right but overestimates the excitation energy of the ^1L_b state by over 3000 cm^{-1}.

We assigned the S_1 state as being ^1L_a, reversing the state ordering in the monomer. There are several arguments for this assignment: (i) the redshifts of the origins increase upon solvation with one and two water molecules,[26] (ii) the total dipole moment is 2.5 times larger in the S_1 state (4.23 D) than in the S_2 state (1.66 D); and (iii) the orientation of the transition dipole moment shows that the S_1 state is a mixture of the ^1L_a and ^1L_b states and the S_2 state is a nearly pure ^1L_b state. The finding is in contrast with the systems indole and indole water. In both systems, the S_1 state does not undergo state reversal upon microsolvation.[27,28] One has to keep in mind that the nomenclatures ^1L_a and ^1L_b only hold strictly for molecules with at least C_2 symmetry.[29,30]

TABLE II. MP2/cc-pVDZ calculated anharmonic ground-state vibrational frequencies and description of the motions. All frequencies are given in cm^{-1}. The numbering follows the nomenclature of Varsanyi (Ref. 23) for ortho-di-light-substituted benzene derivatives, completed for vibrations of the five-membered ring (Ref. 12) and the intermolecular modes (Ref. 22).

Assignment	calc.	Obs.	Obs./calc.	Assignment	calc.	Obs.	Obs./calc.
ρ_1	64	⋯	⋯	18*a*	1043	⋯	⋯
β_1	131	120	0.92	18*b*	1062	1051	0.99
σ	174	157	0.90	δCH	1102	⋯	⋯
10*a*	219	⋯	⋯	18*a*	1124	⋯	⋯
10*b*	237	⋯	⋯	9*a*	1216	1188	0.98
ρ_2	232	182	0.78	3	1238	⋯	⋯
τ	330	⋯	⋯	δNH	1312	⋯	⋯
4*a*	424	⋯	⋯	δNH	1340	⋯	⋯
9*b*	425	430	1.01	δNH	1424	⋯	⋯
6*a*	554	553	1.00	19*b*	1427	1407	0.99
4*b*	574	⋯	⋯	δCHδNH	1466	⋯	⋯
16*a*	590	⋯	⋯	19*a*	1498	⋯	⋯
6*b*	615	622	1.01	δCHδNH	1511	⋯	⋯
CH(inversion)	703	⋯	⋯	8*a*	1593	⋯	⋯
16*b*	760	⋯	⋯	8*b*	1616	⋯	⋯
β_2	712	⋯	⋯	δH_2O	1661	⋯	⋯
1	735	764	1.04	νCH	3087	⋯	⋯
11	780	⋯	⋯	νCH	3089	⋯	⋯
NH(inversion)	771	⋯	⋯	νCH	3115	⋯	⋯
CH(inversion)	821	⋯	⋯	νCH	3154	⋯	⋯
12*a*	894	⋯	⋯	νCH	3172	⋯	⋯
12*b*	898	⋯	⋯	νNH	3289	3412[a]	1.03
5	900	⋯	⋯	νOH_{bond}	3455	3369[a]	0.98
17*b*	941	⋯	⋯	νOH_{free}	3716	3716[a]	1.00

[a]Reference 9.

The Kohn-Sham orbitals that are involved in the two lowest $\pi\pi^*$ transitions are shown in Fig. 2. The squares (weights) of the Configuration Interaction (CI) coefficients of the excitations to ^1L_a and ^1L_b are depicted in Fig. 2. The transition to ^1L_a has a large contribution from excitation from orbital 31 to 32 (weight of 0.95). The dominant excitations of the ^1L_b state take place from orbital 30 to 32 (weight of 0.56), from orbital 31 to 32 (weight of 0.28), and from orbital 31 to 33 (weight of 0.11).

B. Automated assignment of the rotational-resolved spectrum using a genetic algorithm approach

The reliability of the Franck-Condon analysis can be improved considerably, if the changes of the rotational constants upon electronic excitation are known from rotationally resolved electronic spectroscopy.[5] Unfortunately, the absorption of the 7-azaindole-water cluster is well outside the range of our high-resolution laser-induced fluorescence (LIF) experiment. Nakajima *et al.* presented the LIF spectrum of the cluster with a resolution of 300 MHz ($0.01\ cm^{-1}$).[8] This resolution is not sufficient to completely resolve single rovibronic lines. Nevertheless, the band contour can be fitted to a rovibronic Hamiltonian. Due to the absence of single rovibronic lines, a conventional line position assigned fit cannot be performed. Other nonlinear fitting procedures which do not rely on prior assignments suffer from the fact that most of them are local optimizers and the final result depends considerably on the choice of starting parameters. Recently, the use of a genetic-algorithm-(GA) based automated fitting has been improved, so that automated fits also of overlapping and entangled spectra are facilitated. Details can be found in Refs. 31 and 32 and the original literature about the theory of genetic algorithms cited therein. The molecular parameters to be fitted are binary coded, each parameter representing a

TABLE III. CASSCF, TDDFT, and CASPT2 vertical and adiabatic excitation energies given in cm^{-1}.

	CASSCF(10,9)/cc-pVDZ		Expt.
	Vertical	Adiabatic	
$S_1 \leftarrow S_0$	38 238	37 320	33 340
$S_2 \leftarrow S_0$	45 091	⋯	
	CASPT2(10,9)/cc-pVDZ[a]		Expt.
	Vertical	Adiabatic	
$S_1 \leftarrow S_0$	34 808	32 436	33 340
$S_2 \leftarrow S_0$	37 363		
	TDDFT B3LYP/cc-pVTZ		Expt.
	Vertical	Adiabatic	
$S_1 \leftarrow S_0$	35 906	32 360	33 340
$S_2 \leftarrow S_0$	39 001	37 809	
	CASPT2(10,9)/cc-pVDZ[b]		Expt.
	Vertical	Adiabatic	
$S_1 \leftarrow S_0$	34 749	34 114	33 340
$S_2 \leftarrow S_0$	37 110	35 415	

[a]Calculated on the relaxed CASSCF geometries.
[b]Calculated on the relaxed (TD)DFT geometries.

TABLE IV. Molecular constants of 7AI water from the GA fit of the LIF spectrum of Ref. 8 compared to the results of *ab initio* and (TD)DFT calculations. Doubly primed parameters refer to the electronic ground state, while singly primed to the electronically excited state. $\Delta A = A' - A''$, etc. $\Delta\Delta I = \Delta I' - \Delta I''$. All other parameters are defined in the text.

	Expt.	MP2	B3LYP	CAS(10,9)	CIS-HF
A''/MHz	1751	1784	1775	1780	1790
B''/MHz	1336	1333	1349	1288	1302
C''/MHz	759	764	768	749	755
$\Delta I''$/u Å^2	−1.05	−0.92	−1.31	−1.56	−1.11
T_1/K	1.5	⋯	⋯	⋯	⋯
T_2/K	2.1	⋯	⋯	⋯	⋯
w	0.01	⋯	⋯	⋯	⋯
θ/°	±16	⋯	−17	−89	⋯
ΔA/MHz	+33	⋯	+25	−13	+34
ΔB/MHz	+20	⋯	+15	−22	−13
ΔC/MHz	+11	⋯	+9	−10	+2
$\Delta\Delta I$/u Å^2	0.35	⋯	0.45	0.23	−0.42

gene. A vector of all genes which contains all molecular parameters is called a chromosome. In an initial step the values of all parameters are set to random values between lower and upper limits which are chosen by the user. The quality of the solutions then are evaluated by a fitness function. A proper choice of this fitness function is of vital importance for the success of the GA convergence. In Refs. 31 and 32 the fitness function F_{fg} has been defined as

$$F_{fg} = \frac{(\mathbf{f},\mathbf{g})}{\|\mathbf{f}\|\|\mathbf{g}\|}. \tag{2}$$

Here $\mathbf{f}$ and $\mathbf{g}$ are the vector representations of the experimental and calculated spectra, respectively. The inner product $(\mathbf{f},\mathbf{g})$ is defined with the metric $\mathbf{W}$ which has the matrix elements $W_{ij}\ w|j\ i|\ w(r)$ as

$$(\mathbf{f},\mathbf{g}) = \mathbf{f}^{\mathbf{T}}\mathbf{W}\mathbf{g}, \tag{3}$$

and the norm of $\mathbf{f}$ as $\|\mathbf{f}\| = \sqrt{(\mathbf{f},\mathbf{f})}$, similar for $\mathbf{g}$. For $w(r)$ we used a triangle function[31] with a width of the base of Δw,

$$w(r) = \begin{cases} 1 - |r|/\left(\frac{1}{2}\Delta w\right), & \text{for } |r| < \frac{1}{2}\Delta w \\ 0, & \text{otherwise.} \end{cases} \tag{4}$$

One optimization cycle, including evaluation of the fitness of all solutions, is called a generation. Pairs of chromosomes are selected for reproduction and their information is combined via a crossover process. Since crossover combines information from the parent generations, it basically explores the error landscape. The value of a small number of bits is changed randomly by a mutation operator. For the simulation of the rovibronic spectra a rigid asymmetric rotor Hamiltonian was employed.[33]

The temperature dependence of the intensity is described by a following two-temperature model.[34]

$$n(T_1,T_2,w) = e^{-E/kT_1} + we^{-E/kT_2}, \tag{5}$$

where E is the energy of the lower state, k is the Boltzmann constant, w is a weighting factor, and T_1 and T_2 are the two temperatures. Furthermore the angle θ of the transition dipole moment and the inertial a axis were fitted. All relevant parameters for the intensity of the spectrum are presented in Table IV.

The fit of the LIF spectrum described in Ref. 8 was performed using the rotational constants of the ground state from Hartree-Fock calculations and fitting only the excited-state constants. Since the cluster structure in the electronic ground state is largely determined by correlation effects, that are not covered by the Hartree-Fock (HF) theory, we decided to reanalyze the spectrum using the automated GA method. Hereby, we also fitted the rotational constants of the ground state. Figure 3 shows the experimental spectrum and the best fit, using the rotational constants, given in Table IV.

The search space for the ground-state rotational constants has been set to ±100 MHz around inertial parameters that have been obtained from a preliminary B3LYP calculation. The changes of the rotational constants upon electronic excitation were varied by ±50 MHz about a zero change. The angle θ was allowed to vary between 0° (pure a-type) and 90° (pure b-type). As the GA generates the first generation randomly in the limits of the search space, all parameter values within these limits are equally probable. Nevertheless

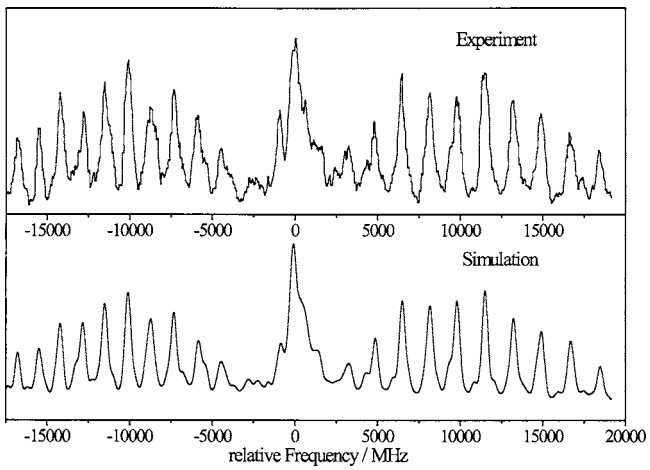

FIG. 3. Comparison of the experimental LIF spectrum of the electronic origin of the 7AI-water cluster with the best fit using the molecular parameters from Table IV.

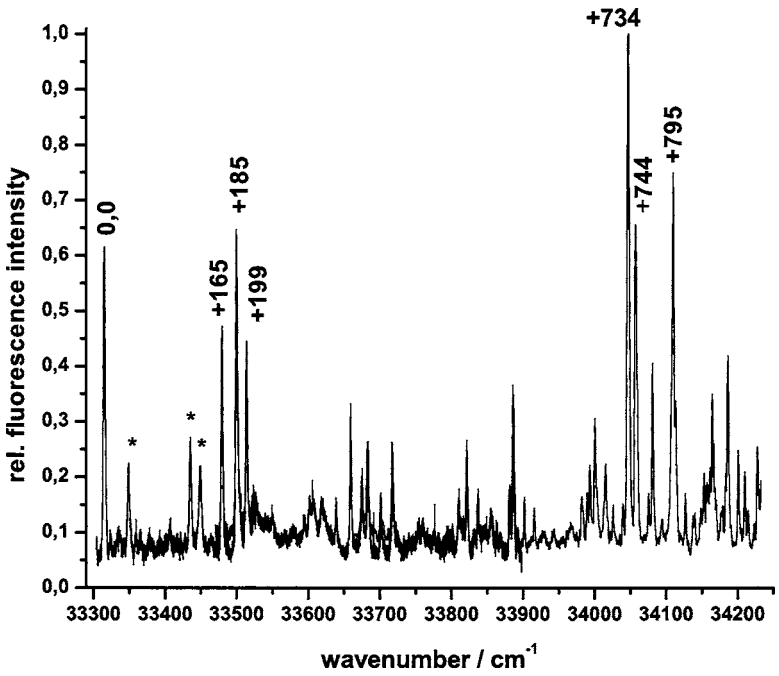

FIG. 4. Fluorescence excitation spectrum of 7AI-water cluster in the region between 33 300 and 34 300 cm^{-1}.

the GA optimizer locates the values of the ground-state parameters very close to those determined by a MP2/cc-pVDZ calculation. This is a good indicator that the GA indeed found the global minimum. Another evidence for the correctness of the fit can be found in the inertial defects. For a planar molecule the inertial defect is expected to be zero or slightly positive. Negative values arise from out-of-plane contributions to the structure. For the rotational constants given in megahertz the inertial defect (in u $Å^2$) is calculated from $\Delta I = 505\,379(1/C - 1/A - 1/B)$. Without any constraints in the fit the ground-state inertial defect matches very closely the value of about 1 u $Å^2$, that is expected from the out-of-plane hydrogen atom of the water moiety.

The normal procedure in a line position assigned fit would be to determine the accuracies of the parameters from the deviation observed from predicted lines. As no single rovibronic lines are resolved, this is impossible here. Instead, we repeat the GA fit several times with different starting generations that are randomly generated. The so-determined standard deviations of the parameters may serve as a measure of the reliability of the fit, but should in no way be identified with the properly determined uncertainties of the fit parameters. From these standard deviations we conclude that the ground-state rotational constants should be correct within 10 MHz and the changes upon electronic excitation within 1 MHz. The so-determined parameters will be used in the subsequent Franck-Condon analysis.

C. Excitation and emission spectra

Figure 4 shows the fluorescence excitation spectrum of the 7AI-water cluster in the region between 33 300 and 34 200 cm^{-1}. The bands marked with an asterisk are due to higher water cluster, cf. Ref. 7.

The labeled peaks in this spectrum were excited to obtain the DF spectra that are shown in Figs. 5–7. The assignment of these absorption bands to specific vibrational modes in the excited state was made on the basis of the propensity rule from the intensities in the emission spectra and are given in the insets of Figs. 5 and 6. The assignment will be explained below, together with a discussion of the respective ground state vibrations, cf. Table VI.

Trace (a) in Fig. 7 shows the emission spectra arising by excitation of $0,0+734$ cm^{-1}. The most intense bands in this spectrum belong to intermolecular modes such as β_1 and σ. Some ring modes can be assigned ($6b$ and 1) as well as combination bands of the modes with intermolecular vibrations. Therefore we suggest that this spectrum arises from excitation of a combination band, possibly $6b+\sigma$. The second trace depicts the emission spectrum, obtained by excitation of $0,0+744$ cm^{-1}. This spectrum consists of rather few bands, thus making the assignment of the excitation band very uncertain.

The first trace of Fig. 5 shows the fluorescence emission spectrum, obtained via excitation of the vibrationless origin 0,0. The assignments given in Figs. 5 and 6 are based on the *ab initio* calculations described in Sec. III A. The calculated frequencies for the ground-state vibrations that were used for the assignment are summarized in Table II. The strongest band in the emission spectrum after excitation at $0,0+165$ cm^{-1} [trace (d) of Fig. 5] is found at 120 cm^{-1} and can be assigned on the basis of anharmonic MP2/cc-pVDZ calculations to the intermolecular β_1 vibration. The corresponding computed frequency value from the MP2 calculation is quite close (131 cm^{-1}) (see Table II). The β_1 mode can be described as an in-plane wag mode of the water moiety with respect to the 7AI moiety. A progression of this mode can be seen up to the third overtone as well as combination bands with the vibrations σ, $6b$, and 1. The assignment of the 165 cm^{-1} band in the absorption spectrum to β_1 in the S_1 state therefore appears reasonable. Excitation at 185 cm^{-1} [trace (g) of Fig. 5] results in a long progression up to the third overtone of a band at 157 cm^{-1} and combination bands with the modes β_1, ρ_2, $6b$, and 1. The MP2 calculations

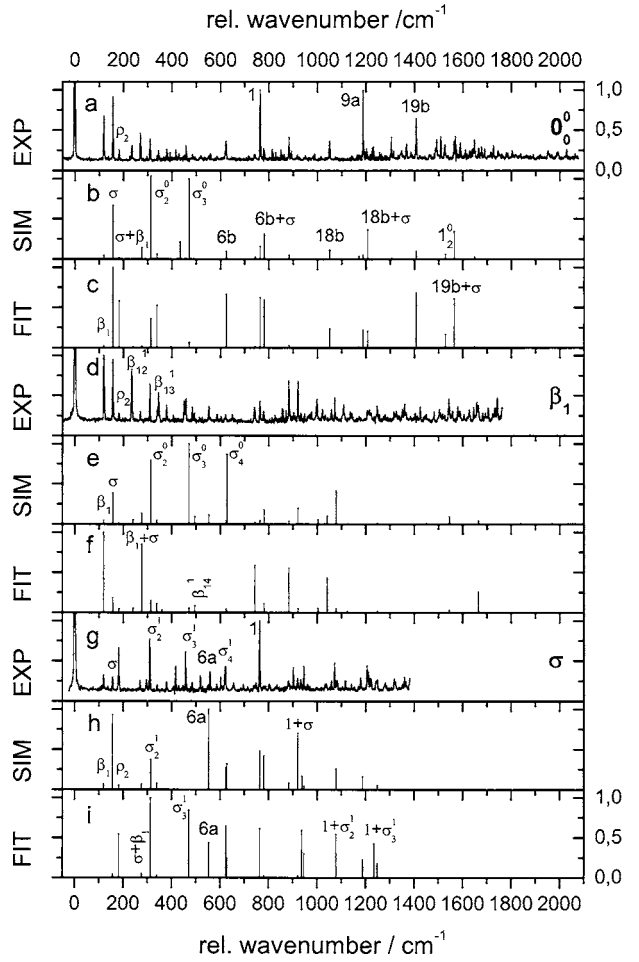

FIG. 5. Fluorescence emission spectra of 7AI-water cluster pumped via $0,0$, $0,0+165$, and $0,0+185$ cm^{-1}.

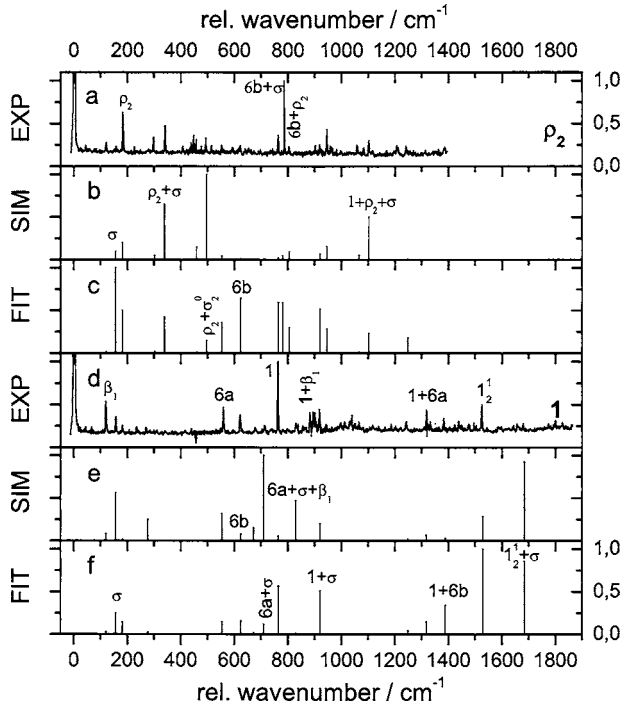

FIG. 6. Fluorescence emission spectra of 7AI-water cluster pumped via $0,0+199$ and $0,0+795$ cm^{-1}.

allow a straightforward assignment of the S_1 vibration at 185 cm^{-1} to mode σ. Upon excitation of $0,0+199$ cm^{-1} the emission spectrum shows a very strong feature at 182 cm^{-1} and combinations with this band [trace (a) of Fig. 6]. Comparison with the results of MP2 calculations show that this band can be assigned to the intermolecular vibration ρ_2. This mode can be described as a wag mode of the out-of-plane hydrogen. Also in this case, the propensity rule allows for an unequivocal assignment of the transition at 199 cm^{-1} to the intermolecular mode ρ_2 in the S_1 state. The strongest band after excitation at $0,0+795$ cm^{-1} [trace (d) of Fig. 6] is located at 764 cm^{-1} and can be assigned to the ring breathing mode 1. The corresponding value obtained via the *ab initio* calculation is 735 cm^{-1}. Furthermore, the overtone of mode 1 as well as many combination bands can be assigned. These findings result in the assignment of the band $0,0+795$ cm^{-1} to mode 1.

The intensities of the emission bands after excitation of the described S_1-state vibrations are summarized in Table V. They show clearly how the strongest transition (marked by an asterisk) appears upon excitation of the corresponding vibration in the excited state, illustrating the propensity rule.

D. Determination of the structure

The change of a molecular geometry upon electronic excitation can be determined from the intensities of absorption or emission bands using the FC principle. The fit procedure has been explained in detail in a previous publication.[5] In a first step the geometry and Hessian matrix of both the ground and excited states are calculated at the TDDFT level (B3LYP/cc-pVTZ). Using the recursion formula given by Doktorov *et al.*[3,4] the Franck-Condon factors[35] of the observed and assigned transitions are calculated and a simulated intensity distribution is obtained. In subsequent steps, the S_1-state geometry is displaced along selected normal coordinates and the resulting intensity pattern is calculated. The displacements are iterated until the observed intensity pattern matches the simulated one. If experimental data for rotational constants in both states are available (possibly for several isotopomers) their changes upon electronic excitation can be used as an additional part of the overall FC fit. The fit has been performed using the program FCFII, which has been developed in our group and described previously.[5] The use of a selected subensemble of normal modes as basis for the displacements is forced by the difficulty to assign a sufficient number of vibrations in the electronically excited state. This selection has to be performed carefully, in order to avoid artificial displacement effects by consideration of too similar modes.

Emission spectra have been obtained from excitations of 0,0, β_1, σ, ρ_2, and 1. These modes were taken as displacement vectors for the fit. Additionally, the ring modes 6*b* and 18*b* were included in the fit. The mode 6*b* shows up in all emission spectra and the 18*b* vibration shows up very prominent in the emission spectrum of the 0,0 transition. Thus, the six motions which form the basis for the displacements upon electronic excitation are β_1, σ, ρ_2, 6*b*, 1, and 18*b*. All of them are intermolecular or in-plane modes and are depicted in Fig. 8.

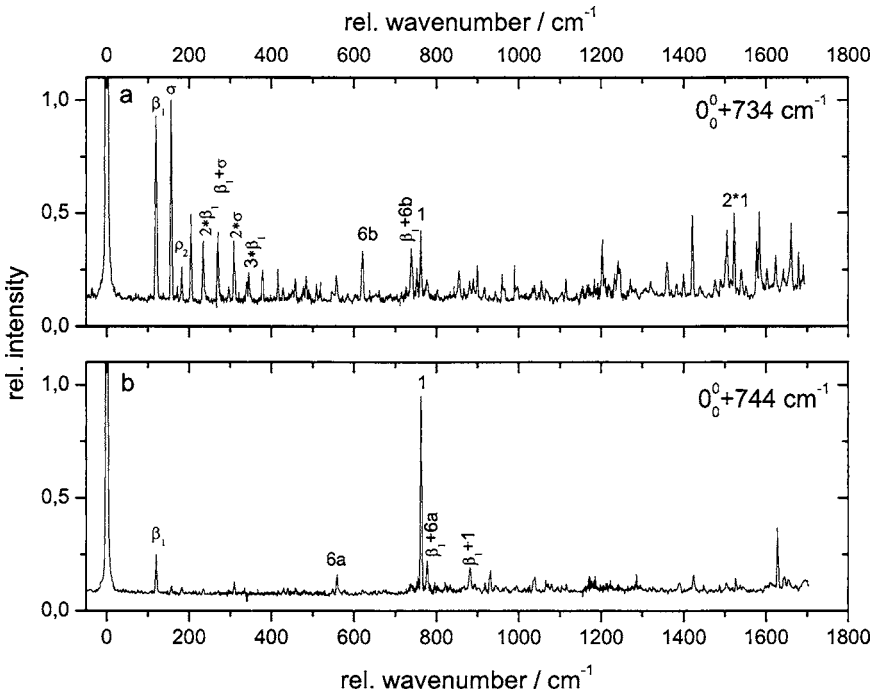

FIG. 7. Fluorescence emission spectra of 7AI-water cluster pumped via 0,0 +734 and 0,0+744 cm^{-1}.

First of all, a simulation of the intensities of the emission bands was performed, using the geometries and the Hessian matrices from the TDDFT B3LYP/cc-pVTZ calculations. We decided to take the results from the (TD)DFT calculations because the CASSCF wave function cannot properly describe the intermolecular bonds due to the lack of dynamic electron correlation. DFT calculations give more reliable structures because a correlation functional is contained in the B3LYP functional. Hence CASSCF underestimates the bond strength between the chromophore and the water molecule resulting in too long bond lengths for the hydrogen bonds. Additionally the rotational constants for the ground state obtained via CASSCF are not particularly good, see especially the rotational constant B, in Table I. From this it follows that the changes in the rotational constants are described poorly on the CASSCF level, cf. Table VII. The simulations from the (TD)DFT calculations are shown in the traces which follow the respective experimental emission spectrum in Figs. 5 and 6. Although the overall performance of these simulations seems not to be too bad, there are severe deviations between the experimental and simulated intensities.

TABLE V. Intensities of emission bands relative to the most intense nonexcitation band of the same spectrum after excitation of different S_1 vibrations. The transition marked with an asterisk is the strongest transition in the respective emission spectrum and is utilized to identify the S_1 mode used for excitation.

	S_1-state transition				
	0,0	0,0+165	0,0+185	0,0+199	0,0+795
β_1	0.6334	1.0000*	0.3064	0.2608	0.5123
σ	0.8654	0.9554	0.2822*	0.2147	0.3399
ρ_2	0.2478	0.2828	0.6274	0.5988*	0.2431
σ_2^0	0.3734	0.6585	0.7437*	0.0000	0.0000
1	1.0000	0.4560	1.0000	0.3651	1.0000*

In the emission spectrum via the excitation of 0,0 the intensity of mode 1 is underestimated, while the intensities of the overtones of σ are strongly overestimated. The largest deviations are observed for the spectrum obtained after the excitation of mode 1. In the simulation the intensity of the combination bands $6a+\sigma$ and $1\frac{1}{2}+\sigma$ are strongly overestimated. Both bands are more intensive in the simulation than the pumped band 1. The experimental trace, however, shows a completely different situation, with weak $6a+\sigma$ and $1\frac{1}{2}+\sigma$ combination bands and 1 as the strongest transition.

After the simulations with unchanged geometries, we

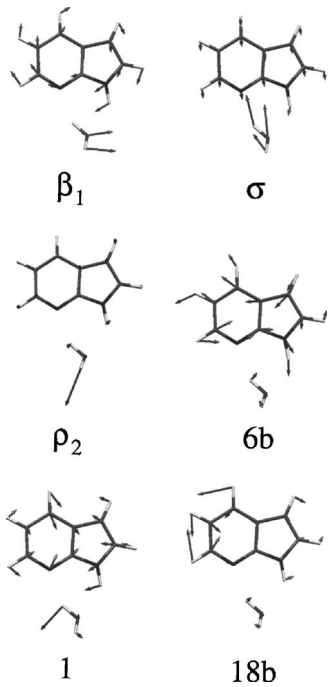

FIG. 8. Normal modes that are used as basis for the structure fit in the electronically excited state.

TABLE VI. Experimental and calculated ground-state vibrational frequencies and assignments of the motions. All frequencies are given in cm^{-1}.

Expt.	MP2	Assignment	Expt.	MP2	Assignment
120	131	β_1	884	862	β_1+1
157	174	σ	920	907	$\sigma+1$
182	232	ρ_2	1033	1038	$\beta_1+\sigma+1$
235	258	β_{12}^0	1051	1062	$18b$
270	300	$\beta_1+\sigma$	1073	1077	σ_2^0+1
310	344	σ_2^0	1103	1139	$\rho_2+\sigma+1$
341	405	$\sigma+\rho_2$	1110	1120	β_{13}^0+1
345	382	β_{13}^0	1165	1192	β_1+18b
393	432	$\beta_{12}^0+\sigma$	1188	1216	$9a$
416	475	$\beta_1+\sigma_2^0$	1203	1235	$\sigma+18b$
430	425	$9b$	1221	1251	σ_3^0+1
459	511	σ_3^0	1247	1231	$6b_2^0$
603	675	σ_4^0	1305	1347	β_1+9a
624	615	$6b$	1407	1427	$19b$
743	746	β_1+6b	1526	1456	1_2^0
764	735	1	1543	1525	$\sigma+6b+1$
779	790	$\sigma+6b$	1658	1652	$\beta_1+\sigma+6b+1$

performed FC fits of the intensities of the vibrations, overtones, and combination bands in the spectra of Figs. 5 and 6 by displacing the S_1-state geometry along the six normal modes described above. The results are shown in the traces, which follow the respective FC simulations in Figs. 5 and 6. Close inspection of all emission spectra shows that the intensity pattern is well reproduced upon displacement of the S_1 geometry. As a representative example let us compare the experimental spectrum, the simulation, and the fit of the emission spectrum upon σ excitation [Fig. 5, traces (g)–(i)]. The intensities of the first and the second overtones of mode σ are too weak in the simulation, what is corrected in the fit. The fundamental of this mode is overestimated in the simulation and is corrected by the fit as well. Also the quality of the simulation of the σ progression is quite bad. The experimental spectrum shows a maximum intensity at the first overtone, while the fundamental of the σ mode is calculated to be the strongest band of this progression in the simulation. An obvious improvement concerns the intensity of mode $6a$, c.f. trace (g) in Fig. 5, for example. In the simulation this band is much too strong, compared with the experimental spectrum. The coupling of the ring breathing mode 1 to mode σ and its overtones is described wrong. The simulation shows a maximum intensity of the fundamental of mode σ whereas the experiment exhibits the maximum at the first overtone. All these intensities are very well reproduced in the FC fit of the σ emission spectrum, cf. Fig. 5, trace (i).

TABLE VII. Comparison of the geometry changes of 7AI and its water cluster upon electronic excitation from our previous work (Ref. 10), from a CASSCF(10,9) study, from a (TD)DFT/B3LYP study, and from the Franck-Condon fit described in the text. All bond-length changes are given in pm.

	FC fit 7AI[a]	CAS(10,9)	B3LYP	FC fit 7AI water	Expt.
H1–O8	···	−2.9	−17.6	−11.5	
N7–H7	···	−3.2	−13.8	−5.4	
N1–C2	+1.3	+1.5	−5.3	−5.7	
C2–C3	+1.5	+1.3	+5.9	+5.9	
C3–C3*a*	−1.5	−1.1	+2.1	+0.3	
C3*a*–C7*a*	+4.5	+4.0	−5.1	−6.9	
C7*a*–N1	−0.8	−1.2	+6.3	+5.4	
C3*a*–C4	+2.0	+2.2	+2.5	+0.7	
C4–C5	+5.0	+4.7	+3.6	+2.4	
C5–C6	+3.6	+3.7	−2.3	−4.6	
C6–N7	+3.5	+3.4	+5.3	+3.8	
N7–C7*a*	+1.4	+1.4	+1.9	±0.0	
Fivering (mean)	+1.0	+0.9	+0.8	−0.2	
Sixring (mean)	+3.3	+3.2	+1.0	−0.8	
ΔA/MHz	−185	−13	+25	+33	+32.9
ΔB/MHz	+0.1	−22	+15	+20	+20.2
ΔC/MHz	−17	−10	+9	+13	+11.3

[a]Reference 10.

Table VII shows the results for the S_1 displacement obtained from the Franck-Condon fit described above. The first column gives the results for the geometry changes from the 7AI monomer obtained from the Franck-Condon fit as discussed in an earlier paper.[10] The second and third columns present the results for the geometry changes upon electronic excitation as obtained from the CASSCF and (TD)DFT/B3LYP calculations. The fourth column shows the results for the geometry changes from the Franck-Condon fit to 105

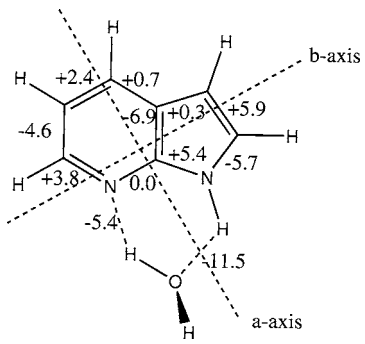

FIG. 9. Schematic drawing of the geometry changes in 7AI-water cluster upon electronic excitation.

fluorescence emission bands and to the changes of the rotational constants of one isotopomer of 7AI-water cluster. The fifth column gives the experimentally determined rotational constant changes.

IV. CONCLUSIONS

The geometry changes of 7AI water upon electronic excitation are displayed in Fig. 9. The main changes of the 7AI-water geometry can be described as a distinct shortening of both the O···H and the H···N hydrogen bonds (−11.5 and −5.4 pm, respectively). This reasoning follows directly from the experimental finding that most of the Franck-Condon active vibrations are intermolecular ones, both in absorption as well as in emission. While for the monomer the pyridine ring expands and the pyrrole ring distorts unsymmetrically upon electronic excitation, the situation is different for the cluster. Here, both moieties are distorted unsymmetrically, cf. Table VII. This deformation of the pyridine moiety in the cluster can be described as a shortening of the C3*a*–C7*a* (−4.6 pm) and the C5–C6 bonds (−6.9 pm) with minor changes of the remaining bonds, while the deformation of the pyrrole moiety is characterized by a shortening of the N1–C2 bond (−5.7 pm) and the C3*a*–C7*a* (−6.9 pm) bonds and a lengthening of the C2–C3 (+5.9 pm) and the C7*a*–N1 (+5.4 pm) bonds.

The *ab initio* calculated geometry changes are qualitatively correct but could be improved significantly by the Franck-Condon fit. Of course, only transitions that are assigned to a particular normal mode without any doubt can be used for the determination of the distortion upon electronic excitation. Therefore, the quality of the fitting procedure is limited by the number of observed and assigned normal modes. Additionally, the rotational constant changes from the LIF spectrum exhibit larger standard deviations than usual, because the measured LIF spectrum is not resolved into individual rovibronic lines.

The changes in the 7AI moiety upon electronic excitation of the cluster can be deduced from the respective molecular orbitals. As can be seen from Fig. 2, the main effect of the electronic excitation to the ^1L_a state is a shift of the electron density from the pyrrole ring to the pyridine ring. The excitation transfers electron density from nonbonding to bonding orbitals in the six-membered ring (C3*a*–C7*a* and C5–C6), in good agreement with the experimentally observed geometry changes. The electronic density distribution in the aromatic ring system upon electronic excitation of the cluster is very different compared with the monomer. The spectrum fit of the monomer shows an approximately symmetric ring expansion and the coefficients of the involved molecular orbitals reflect this experimental findings.[10] Obviously, the association with water leads to a severe distortion of the electron-density distribution in the aromatic ring system. An excitation nonbonding → antibonding is predominant for the remaining bonds in the pyridine ring and therefore leads to a bond lengthening. In the pyrrole ring the main effect is the transfer of electron density from bonding to nonbonding orbitals, thus leading to the observed bond order loss (C2–C3 and C7*a*–N1) in the five-membered ring.

To conclude, we find changes of the monomer geometry upon electronic excitation in the azaindole-water cluster which are very different from the changes in the photoexcited monomer itself. This experimental finding is supported by *ab initio* geometry optimizations of the azaindole geometry in the monomer and in the water cluster, using time-dependent density-functional theory with the B3LYP functional. Also the theory predicts here completely different geometry changes in the azaindole moiety. Therefore, the conventional notion of only slightly modified monomer moieties in a cluster has no general validity and should be reconsidered in each individual case.

ACKNOWLEDGMENTS

The financial support of the Deutsche Forschungsgemeinschaft (KL531/22-1) is gratefully acknowledged. This work is part of the Ph.D. thesis of one of the authors (R.B.).

[1] C. Ratzer, J. Küpper, D. Spangenberg, and M. Schmitt, Chem. Phys. **283**, 153 2002.
[2] F. Duschinsky, Acta Physicochim. URSS **7**, 551 1937.
[3] E. V. Doktorov, I. A. Malkin, and V. I. Man'ko, J. Mol. Spectrosc. **56**, 1 1975.
[4] E. V. Doktorov, I. A. Malkin, and V. I. Man'ko, J. Mol. Spectrosc. **64**, 302 1977.
[5] D. Spangenberg, P. Imhof, and K. Kleinermanns, Phys. Chem. Chem. Phys. **5**, 2505 2003.
[6] S. K. Kim and E. R. Bernstein, J. Phys. Chem. **94**, 3531 1990.
[7] K. Fuke, H. Yoshiuchi, and K. Kaya, J. Phys. Chem. **88**, 5840 1984.
[8] A. Nakjima, M. Hirano, R. Hasumi, K. Kaya, H. Watanabe, C. C. Carter, J. M. Williamson, and T. Miller, J. Phys. Chem. A **101**, 392 1997.
[9] H. Yokoyama, H. Watanabe, T. Omi, S. Ishiuchi, and M. Fujii, J. Phys. Chem. A **105**, 9366 2001.
[10] R. Brause, M. Schmitt, D. Krügler, and K. Kleinermanns, Mol. Phys. **102**, 1615 2004.
[11] M. Schmitt, U. Henrichs, H. Müller, and K. Kleinermanns, J. Chem. Phys. **103**, 9918 1995.
[12] W. Roth, C. Jacoby, A. Westphal, and M. Schmitt, J. Phys. Chem. A **102**, 3048 1998.
[13] M. Frisch, G. W. Trucks, H. B. Schlegel *et al.*, GAUSSIAN 03, revision b.04 (Gaussian, Inc., Pittsburgh, PA, 2003).
[14] T. H. Dunning, Jr., J. Chem. Phys. **90**, 1007 1989.
[15] O. Treutler and R. Ahlrichs, J. Chem. Phys. **102**, 346 1995.
[16] M. von Arnim and R. Ahlrichs, J. Comput. Chem. **19**, 1746 1998.
[17] F. Furche and R. Ahlrichs, J. Chem. Phys. **117**, 7433 2002.
[18] P. Deglmann, K. May, F. Furche, and R. Ahlrichs, Chem. Phys. Lett. **384**, 103 2004.
[19] P. Deglmann, F. Furche, and R. Ahlrichs, Chem. Phys. Lett. **362**, 511 2002.
[20] P. Deglmann and F. Furche, J. Chem. Phys. **117**, 9535 2002.
[21] G. Karlström, R. Lindh, P.-Å. Malmqvist *et al.*, Comput. Mater. Sci. **28**, 222 2003.
[22] M. Schütz, T. Bürgi, and S. Leutwyler, J. Chem. Phys. **99**, 3763 1992.
[23] G. Varsanyi, *Assignments for Vibrational Spectra of 700 Benzene Derivatives* (Wiley, New York 1974).
[24] G. Schaftenaar and J. H. Noordik, J. Comput.-Aided Mol. Des. **14**, 123 2000.
[25] S. Portmann, MOLEKEL available from the web at http://www.cscs.ch/molekel/, 2002.
[26] Y. Huang, S. Arnold, and M. Sulkes, J. Phys. Chem. **100**, 4734 1996.
[27] T. Korter, D. Pratt, and J. Küpper, J. Phys. Chem. A **102**, 7211 1998.
[28] C. Kang, T. Korter, and D. Pratt, J. Chem. Phys. **122**, 4301 2005.
[29] J. Platt, J. Chem. Phys. **17**, 484 1949.

[30] E. Heilbronner and J. Murrel, Mol. Phys. **6**, 1 1963.
[31] J. A. Hageman, R. Wehrens, R. de Gelder, W. L. Meerts, and L. M. C. Buydens, J. Chem. Phys. **113**, 7955 2000.
[32] W. L. Meerts, M. Schmitt, and G. Groenenboom, Can. J. Chem. **82**, 804 2004.
[33] H. C. Allen and P. C. Cross, *Molecular Vib-Rotors* (Wiley, New York, 1963).
[34] Y. R. Wu and D. H. Levy, J. Chem. Phys. **91**, 5278 1989.
[35] See EPAPS Document No. E-JCPSA6-123-012545 for all calculated Franck-Condon factors. This document can be reached via a direct link in the online article's HTML reference section or via the EPAPS homepage (http://www.aip.org/pubservs/epaps.html).